Effects of gravity on soot formation in a coflow laminar methane/air diffusion flame

Kong, Wenjun; Liu, Fengshan

Publisher's version / Version de l'éditeur:
https://doi.org/10.1007/s12217-009-9175-z
Microgracity Science and Technology, 22, 2, pp. 205-214, 2009

Microgravity Sci. Technol
DOI 10.1007/s12217-009-9175-z

ORIGINAL ARTICLE

Effects of Gravity on Soot Formation in a Coflow Laminar Methane/Air Diffusion Flame

Wenjun Kong · Fengshan Liu

Received: 22 August 2009 / Accepted: 17 November 2009

Abstract Simulations of a laminar coflow methane/air diffusion flame at atmospheric pressure are conducted to gain better understanding of the effects of gravity on soot formation by using detailed gas-phase chemistry, complex thermal and transport properties coupled with a semiempirical two-equation soot model and a nongray radiation model. Soot oxidation by O_2, OH and O was considered. Thermal radiation was calculated using the discrete ordinate method coupled with a statistical narrow-band correlated-K model. The spectral absorption coefficient of soot was obtained by Rayleigh's theory for small particles. The results show that the peak temperature decreases with the decrease of the gravity level. The peak soot volume fraction in microgravity is about twice of that in normal gravity under the present conditions. The numerical results agree very well with available experimental results. The predicted results also show that gravity affects the location and intensity for soot nucleation and surface growth.

Keywords Soot formation · Coflow diffusion flame · Microgravity combustion

W. Kong (✉)
Institute of Engineering Thermophysics, Chinese Academy of Sciences, PO Box 2706, Beijing 100190, China
e-mail: wjkong@mail.etp.ac.cn

F. Liu
Institute for Chemical Process and Environmental Tech., NRC, Ottawa, Canada

Introduction

A detailed understanding of soot formation and oxidation in flames can lead to improvements in combustion applications and provide findings relevant to fire safety. Thus soot research has received considerable attention in both normal gravity and microgravity (Haynes and Wagner 1981; Glassman 1988; Ku et al. 1995; Haggard and Cochran 1972; Greenberg and Ku 1997a, b; Megaridis et al. 1996; Sunderland et al. 1994; Urban et al. 2000; Konsur and Megaridis 1999; Lin et al. 1999; Aalburg et al. 2005; Walsh et al. 2000; Kaplan et al. 1996a). In microgravity, the elimination of buoyancy-induced flows increases the residence time and decreases the fresh air supply. This microgravity characteristic strongly affects the soot formation processes in general leading to longer, wider and sootier flames than their normal gravity counterparts.

Most studies have focused on experimental investigations on the soot field structures at microgravity (Greenberg and Ku 1997a, b; Megaridis et al. 1996; Sunderland et al. 1994; Urban et al. 2000; Konsur and Megaridis 1999; Lin et al. 1999; Aalburg et al. 2005) to elucidate the effects of buoyancy on soot formation. However, it is difficult to investigate all the aspects that influence soot formation because of the cost and the limited number of experiments that can be conducted in microgravity. Due to the limited weight and space, only a few compact measurement apparatus can be used in microgravity environment leading to limited information from experiment. Thus, modeling the effects of gravity on soot formation is of significant importance for understanding the influences of buoyancy on soot processes and flame structure in general. More recently, Vietoris et al. (2000) and Brahmi et al. (2005)

Published online: 12 December 2009

conducted studies of a diffusion flame established in a non-buoyant laminar flat plate boundary layer, which is closer to a fire scenario aboard a spacecraft. They focused on the visible emission of the flame and showed that for low velocity air flows the luminosity of the flame increased with the oxidizer velocity for both solid (Vietoris et al. 2000) and gaseous (Brahmi et al. 2005) fuels. Legros et al. (2006) extended the above studies to quantify the influence of the oxidizer velocity on soot concentrations showing that increasing the oxidizer velocity enhanced both soot oxidation and soot formation. To provide further evidence on such observations, Fuentes et al. (2007) focused on the soot trajectory in a non-buoyant, laminar, flat plate, boundary layer diffusion flame similar to that of Brahmi et al. (2005). Their results showed that local soot volume fractions are a function of the local formation and oxidation residence times and are not necessarily related to the global residence time. The study in Legros et al. (2009) is an extension of Fuentes et al. (2007) which complements the modelling to allow for a quantitative estimation of the ratio of formation to oxidation characteristic times. The study of Legros et al. (2009) did not aim to produce a model for soot production but to describe the different transport phenomena involved.

Although several studies on numerical simulations of soot formation in jet diffusion flames have been carried out previously (Kaplan et al. 1996a, b; Smooke et al. 1992, 1996; Walsh et al. 1998; Guo et al. 2002; Liu et al. 2002, 2004), the gravitational effects on sooting diffusion flames have not yet been studied in detail except for Kaplan et al. (1996a).

Kaplan et al. (1996a) solved the time-dependent reactive-flow Navier–Stokes equations coupled with a phenomenological chemical reaction model and a fuel based global soot model to investigate the effects of buoyancy on the dynamics and behavior of heavily sooting flames under different gravity conditions. Their results showed that soot production was enhanced greatly at microgravity by as much as a factor of 10. The predicted enhancement in the peak soot volume fraction is much greater than that experimentally measured in drop tower (Greenberg and Ku 1997a; Megaridis et al. 1996). The differences between the computations and the experimental results imply more efforts are needed for simulations of soot formation in microgravity. In the absence of gravity, radiation becomes relatively more important due to the elimination of buoyancy-induced convection, which significantly prolongs the residence time. It is strongly coupled with soot processes through its direct impact on the flame temperature. The oversimplified treatment of radiation by using the optically thin model and the simplified soot model with skeletal gas-phase kinetic mechanisms in Kaplan et al. (1996a) may introduce large error to their results.

Therefore, the purpose of this study is to investigate the effects of buoyancy on soot formation under different levels of gravity by using detailed gas-phase chemistry and complex thermal and transport properties. The effects of soot inception, growth and oxidation on gas-phase chemistry were taken into account. The radiation heat loss was accounted for by the discrete ordinate method (DOM) coupled to a statistical narrow-band correlated-K (SNBCK) model for radiative properties of CO, CO_2, H_2O and soot. This flame model has been verified in previous studies in normal gravity (Guo et al. 2002; Liu et al. 2002, 2004, 2006; Liu and Kong 2008) and will be extended its application scope in this work.

Numerical Method

The investigated flame is a coflow laminar methane/air diffusion flame in which a cylindrical fuel stream is surrounded by an annular coflowing air jet.

In axisymmetric cylindrical coordinates (r; z), the generalized form of the governing equations for gas-phase in low Mach number limit is

$$\frac{\partial}{\partial r}(\rho u_r \phi) + \frac{\partial}{\partial z}(\rho u_z \phi) = \frac{1}{r}\frac{\partial}{\partial r}\left(\Gamma_\phi r \frac{\partial \phi}{\partial r}\right) + \frac{\partial}{\partial z}\left(\Gamma_\phi \frac{\partial \phi}{\partial z}\right) + S_\phi \quad (1)$$

where ϕ is the variable used in the continuity, momentum, species, and energy-conservation equation. ρ, u, Γ_ϕ and S_ϕ are the density of gas-phase, velocity, the transport coefficients and the source terms that appear in the governing equations, respectively. The details for the governing equations can be found in (Guo et al. 2002; Liu et al. 2002, 2004). The gravitational term was included in the momentum equation. The effects of buoyancy on the flame behaviors under various gravitational conditions can be investigated by changing this term. Correction velocities were used to ensure that the mass fractions sum to unity.

The radiation source term in the energy equation was obtained using the discrete-ordinates method in axisymmetric cylindrical geometry. Spatial discretisation of the transfer equation was achieved using the finite volume method along with the central difference scheme for the diffusion term and the exponential scheme for the convection term. A SNBCK based wide band model was employed to obtain the absorption

coefficients of the combustion products containing CO, CO_2 and H_2O at each wide band. The spectral absorption coefficient of soot was obtained by Rayleigh's theory for small particles and assumed to be $5.5 f_v/\lambda$ with f_v being the soot volume fraction and λ the wavelength. The wide bands considered in the calculations were formed by lumping 10 successive uniform narrowbands of 25 cm^{-1}, giving a bandwidth of 250 cm^{-1} for each wide band. The blackbody intensity at each wide band was evaluated at the band centre. The SNB parameters for CO, CO_2 and H_2O were from Soufiani and Taine (1997).

A modified version of the semi-empirical two-equation formulation of soot kinetics was used to model soot nucleation, growth and oxidation. The governing equations for soot mass fraction and number density are as follows.

$$\rho u_r \frac{\partial Y_s}{\partial r} + \rho u_z \frac{\partial Y_s}{\partial z} = -\frac{1}{r}\frac{\partial}{\partial r}\left(r\rho V_{T,r} Y_s\right) - \frac{\partial}{\partial z}\left(\rho V_{T,z} Y_s\right) + S_m \quad (2)$$

$$\rho u_r \frac{\partial N}{\partial r} + \rho u_z \frac{\partial N}{\partial z} = -\frac{1}{r}\frac{\partial}{\partial r}\left(r\rho V_{T,r} N\right) - \frac{\partial}{\partial z}\left(\rho V_{T,z} N\right) + S_N \quad (3)$$

where Y_s is the soot mass fraction and N is the soot number density defined as the particle number per unit mass of mixture. Quantities $V_{T,r}$ and $V_{T,z}$ are the soot thermophoretic velocities in the r and z directions, respectively, and are calculated as

$$V_{T,x_i} = -0.65 \frac{\mu}{\rho T}\frac{\partial T}{\partial x_i} \qquad x_i = r, z \quad (4)$$

The source term S_m in Eq. 2 accounts for the contributions of soot nucleation (ω_n), surface growth (ω_g) and oxidation (ω_O). Therefore,

$$S_m = \omega_n + \omega_g - \omega_o \quad (5)$$

This semi-empirical soot model assumes that C_2H_2 is the only chemical species responsible for soot nucleation and surface growth processes and the corresponding chemical reactions are assumed as:

$$C_2H_2 \rightarrow 2C\,(S) + H_2 \quad (R1)$$

$$C_2H_2 + nC\,(S) \rightarrow (n+2)\,C\,(S) + H_2 \quad (R2)$$

The rates of nucleation and growth are given as

$$R_1 = k_1\,(T)\left[C_2H_2\right], \quad \left(\text{kmol m}^{-3}\,\text{s}^{-1}\right), \quad (6)$$

$$R_2 = k_2\,(T)\,f\,(A_s)\left[C_2H_2\right], \quad \left(\text{kmol m}^{-3}\,\text{s}^{-1}\right), \quad (7)$$

where $f(A_s)$ denotes the functional dependence of soot surface growth on soot surface area per unit volume, and $[C_2H_2]$ is the mole concentration of acetylene.

Soot oxidation by O_2, OH and O was taken into account in the present study, and was assumed the following reactions:

$$0.5O_2 + C\,(S) \rightarrow CO \quad (R3)$$

$$OH + C\,(S) \rightarrow CO + H \quad (R4)$$

$$O + C\,(S) \rightarrow CO \quad (R5)$$

The reaction rates per unit surface area of these three reactions (kg m^{-2} s^{-1}) are given as

$$R_3 = 120\left[\frac{k_A X_{O2}\chi}{1 + k_Z X_{O2}} + k_B X_{O2}\,(1-\chi)\right],$$

$$\chi = \left[1 + \frac{k_T}{k_B X_{O2}}\right]^{-1} \quad (8)$$

$$R_4 = \varphi_{OH} k_4\,(T)\,T^{-1/2} X_{OH} \quad (9)$$

$$R_5 = \varphi_O k_5\,(T)\,T^{-1/2} X_O \quad (10)$$

where X_{O2}, X_{OH} and X_O denote the mole fractions of O_2, OH and O, and φ_{OH} and φ_O are the collision efficiencies for OH and O attacking on soot particles.

The source term S_N in Eq. 3 represents the production and destruction of the number density of soot particles due to nucleation and agglomeration. The soot volume fraction f_v is calculated as $f_v = \rho Y_s / \rho_s$, where ρ_s is the density of soot. Further details of the governing equations, radiation model and soot model can be found in Guo et al. (2002) and Liu et al. (2002).

This simplified soot model, when used in conjunction with the GRI-Mech3.0 mechanism (Smith et al. 2009), has been shown to perform very well in the prediction of a laminar coflow CH_4/air diffusion flame at atmospheric pressure (Liu et al. 2004). In addition, the effect of gravity on soot formation is a physical phenomenon, but not a chemical one. Therefore, it is appropriate to use this simplified soot formation model for the purposes of the present study.

The fully coupled equations were discretized by the finite volume method. SIMPLE algorithm for pressure-velocity coupling was employed. The equations of momentum, pressure correction, temperature, soot mass fraction, and soot number density were solved using the tri-diagonal matrix algorithm. Equations of gas-phase species were solved simultaneously using a direct solver at each control volume. The gas-phase reaction mechanism used in the present calculations was derived from GRI-Mech 3.0, along with recommended thermal and

transport properties. All reactions and species related to NOx formation (except N_2) were removed from the standard GRI-Mech 3.0, resulting in a mechanism consisting of 36 species and 219 reactions.

Results and Discussions

The burner fuel tube had an inner radius of $R_I = 0.545$ cm with a wall thickness of 0.095 cm. The radius of the coflow air was $R_O = 5$ cm. Uniform inlet temperatures were assumed for both the fuel and the air streams: $T_F = 300$ K, $T_A = 300$ K. Uniform inlet coflow air velocity was assigned at $v_A = 77.6$ cm/s. The influences of the coflow air velocities on the flame structure and soot formation at different levels of gravity was discussed in another paper (Kong and Liu 2009), where three coflow air velocities of 77.6, 30, and 5 cm/s were investigated. The results showed that the coflow air velocity had significant effects on the flame structure and soot formation. Thus the effects of coflow velocities will not be discussed here again. This study focused on the case of a coflow velocity of 77.6 cm/s. Non-uniform grids were used in both r and z directions to provide greater resolution in the large gradient regions without an excessive increase in the computing time. Fine grids were placed in the r direction between 0 and 1.2 cm with a grid resolution of about 0.16 mm. Fine grids were used in the burner exit region in the z direction and the grid gradually became coarser as the distance from the burner exit increased. The height of the solution domain was about 8.3 cm. In total, the computational domain was divided into $211(z) \times 125(r)$ control volumes. Inlet conditions were specified for the fuel and air streams at the $z = 0$ boundary. A parabolic laminar pipe flow velocity profile was assigned to the inlet velocity of the fuel stream, i.e., $2v_F\left[1-(r/R_I)^2\right]$, where r is the radial position, R_I is the inner radius of the fuel tube, and v_F is the mean velocity of the fuel. The mean fuel stream velocity was fixed at $v_F = 6.52$ cm/s. For the air stream, a boundary layer velocity profile was assumed inside the boundary layer (formed along the outer surface of the fuel pipe) and the uniform velocity was prescribed outside it. Symmetry conditions were used at the centerline, i.e., $r = 0$. Free slip conditions were assumed for the velocity at the $r = R_O$ boundary. Zero-gradient conditions were enforced at the exit boundary. In the calculation of radiation heat transfer, all the boundaries were assumed to be cold at 300 K and black.

Figure 1 shows the predicted fields of temperature under different gravity levels with the maximum temperature indicated in each case. It is clearly seen from

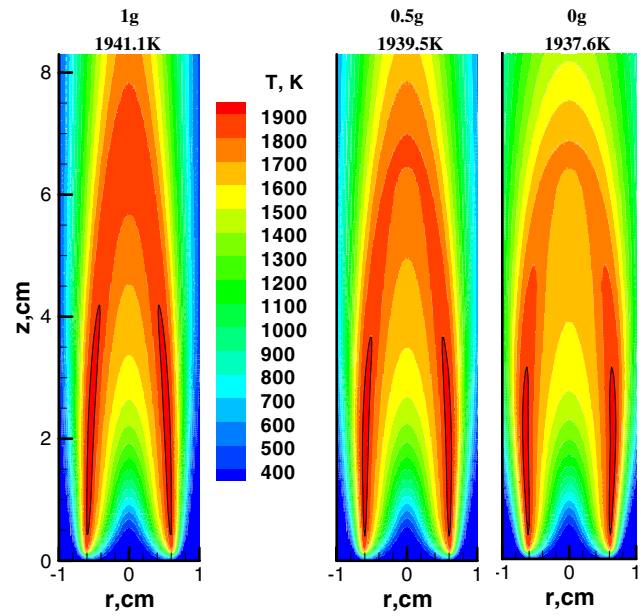

Fig. 1 Comparison of temperature distributions under different gravity levels with the peak values indicated

the results that the highest temperatures in the flames are not at the flame tips, but in the outer annular region lower in the flame at about z = 0.75 to 2.25 cm for normal gravity (1 g) flame, z = 0.75 to 2 cm for partial gravity (0.5 g) flame and z = 0.75 to 1.75 cm for zero gravity (0 g) flame, respectively. The zones of temperature greater than 1900K shown in Fig. 1 were marked by black lines at about z = 0.4 to 4.2 cm for normal gravity (1 g) flame, z = 0.4 to 3.7 cm for partial gravity (0.5 g) flame and z = 0.4 to 3.1 cm for zero gravity (0 g) flame, respectively. Thus, the high-temperature zone becomes shorter when the influence of gravity is removed. This trend is consistent with the results obtained by Walsh et al. (2000). The overall flame temperature distribution for 1 g flame is similar to that computed by Liu et al. (2004) and Smooke et al. (1999). It is also seen from Fig. 1 that the flame high-temperature zone becomes wider as the level of gravity is reduced. The elongated tear-drop like flame tip in normal gravity becomes rounded in microgravity. Since the flame shape depends mainly on the aerodynamic feature of the combustion processes, the change of the flame shape indicates the variation of the velocity fields. This will be explained more later. Again from Fig. 1, it is seen that the maximum temperature decreases with the reduction of the gravity level. The absence of buoyancy-induced flows in microgravity reduces the axial velocity (see below Fig. 3) and increases the reactant residence time and soot growth time. Soot volume fraction is significantly enhanced with decreasing

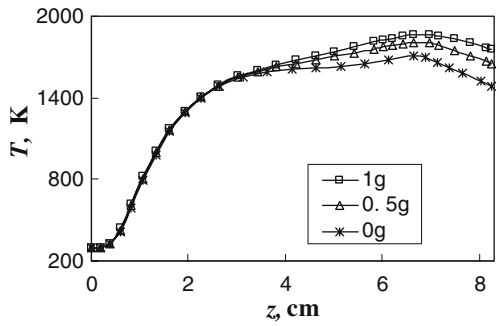

Fig. 2 Temperature distributions along the centerline under different gravity levels

gravity (see below). As a result, the microgravity conditions enhance flame radiation. Thus radiation cooling effect increases with the decrease of the gravity level, leading to reduced flame temperature.

Figure 2 shows the temperature distributions along the centerline under different gravity levels. It is seen that the effects of gravity on flame temperature are mainly in the upper portion of the flame beyond about z = 4 cm, which is due to the relatively high coflow air velocity. In zero gravity radiation becomes relatively more important due to the elimination of buoyancy and more soot is formed due to longer residence time for soot surface growth. As a result, the temperature decreases with the decrease of the gravity level. The increased relative importance of radial heat conduction with decreasing gravity also contributes to the centerline temperature decreases in the upper portion of the flame. It is seen from Fig. 2 that the temperature at z = 8 cm for normal gravity flame is 18% higher than that for zero gravity flame.

Figure 3 shows the axial velocity profiles along the centerline of the flame under different gravity environments. The profiles show significant reduction in axial velocity due to the loss of buoyancy-induced convection. The difference increases with the distance above the burner. The buoyancy-induced velocity is proportion to $(gz)^{0.5}$, which can be derived based on a balance between the buoyancy force and the inertial terms in the momentum equation. Thus, the axial velocities for normal and partial gravity flames increase with the axial height z. While in zero gravity, there is no buoyancy-induced convection, and the transport of combustion products and the supply of fresh air and fuel to the flame front are only by the process of molecular diffusion and the coflow jet momentum. This feature is reflected in Fig. 3 where the axial velocity is almost unchanged as the axial position z is great than about 2.25 cm in zero gravity. Due to the removal of buoyancy-induced convection in the vertical direction, the effect of radial diffusion of species and temperature becomes relatively more important. As a result, the flame becomes wider in zero gravity. Furthermore, it is clearly seen from Fig. 3 that the influences of buoyancy on flame axial velocity can be neglected in the near burner region when the axial position z is less than about 1 cm.

Figure 4 displays the distributions of soot volume fraction at various gravity levels. The profiles of soot volume fraction in Fig. 4 indicate that the visible flame height increases slightly with the decrease of gravity, suggesting the gravity has an insignificant effect on the flame height under the present condition of high coflow air velocity. Anyway the effect of gravity on flame height becomes important with the decrease of the coflow velocity. At low coflow air velocity the

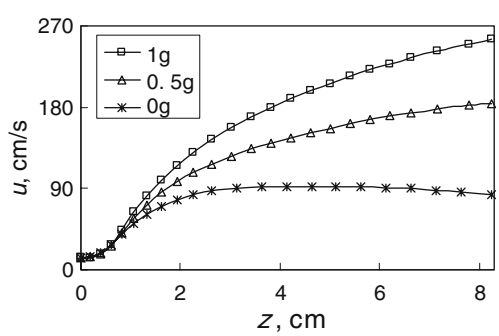

Fig. 3 Axial velocity distributions along the centerline in different gravitational level

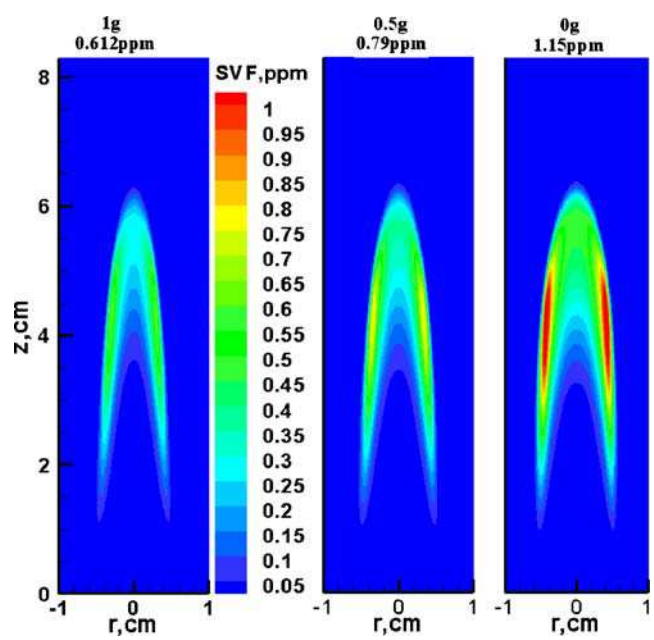

Fig. 4 Comparison of predicted soot volume fraction distributions under different gravity level with the peak values indicated

flame height in microgravity is obviously taller than that at normal gravity (Kong and Liu 2009). This is in qualitative agreement with the experimental results that the observed microgravity flames are taller than their normal gravity counterparts (Bahadori et al. 1990) where the fuel jet is issued into a quiescence environment. The maximum values of soot volume fraction in each case are in the annular region. The area of the annular region in zero gravity flame is greater than that in normal gravity. Therefore, the visible microgravity flame is wider than that in normal gravity, as a result of reduced radially inward flow. The values of soot volume fraction in the annular region increase with the decrease of the gravitational level. Furthermore, the distributions of soot volume fraction in Fig. 4 indicate that the values greater than 0.3 ppm in normal gravity flame lies inside a narrow annular region at about $z = 2.5$ to 5.5 cm with a sharp tip. In contrast, soot volume fraction greater than 0.3 ppm in non-buoyant flame lies in a large region at about $z = 2$ to 6 cm with a rounded tip. As discussed above, the reduction in buoyant force leads to the decrease in the axial velocities in the reduced gravity flames. Therefore, the residence time of soot in non-buoyant flame is longer than that in buoyant flame mainly due to the much lower axial velocities in reduced gravity environment. This is in agreement with the analysis in Sunderland et al. (1994). The predicted peak soot volume fraction in normal gravity is 0.612 ppm, which is reasonably good agreement with the measured maximum of 0.56 ppm for a steady but somewhat larger methane-air coflow diffusion flame (Kaplan et al. 1996b). The predicted maximum soot volume fraction under 0 g is 1.15 ppm which is almost doubled that under 1 g (a factor of 1.9). The drop tower experimental results showed that the maximum soot volume fraction measured at 0 g was nearly a factor of 2 higher than that at 1 g (Greenberg and Ku 1997a; Megaridis et al. 1996). Though the fuel and flow conditions are different in this paper and the literature (Greenberg and Ku 1997a; Megaridis et al. 1996), the same soot enhanced factor of 2 for non-buoyant flames indicates that the present simulation is likely to be more reliable than previous work (Kaplan et al. 1996a). Because of the increase in soot volume fraction and the longer resident time, soot emits larger quantities of thermal radiation in microgravity leading to a lower peak flame temperature shown in Fig. 1.

It is seen from Eqs. 6 and 7 that the rates of soot nucleation and surface growth are only in proportion to the concentration of C_2H_2. As discussed in Fig. 3, the reactant residence time increases with decreasing of gravity. Therefore, gravity affects the distributions of chemical species. To illustrate the effects of gravity on the processes affecting soot, Figs. 5, 6, 7, 8 and 9 show the profiles of soot nucleation, surface growth and oxidation rates with their respective peak values indicated. The different soot volume fraction distributions in the 1 and 0 g flames show significant influences of buoyancy on soot formation, as revealed in Fig. 4. Thus

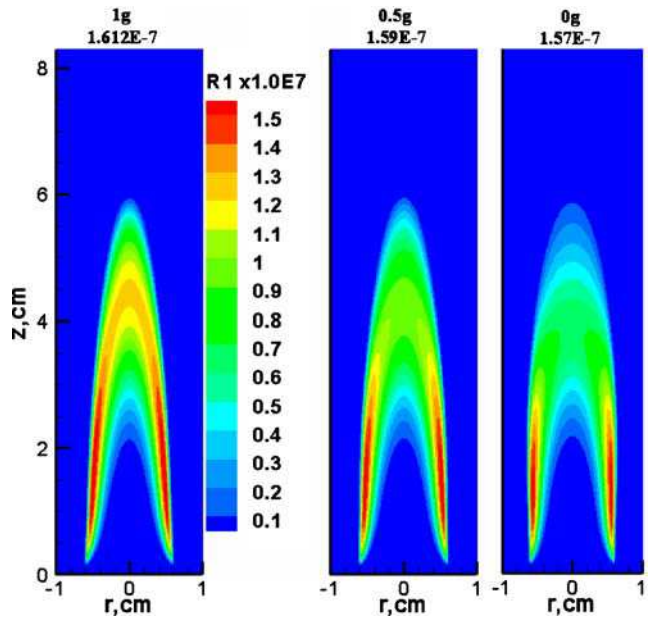

Fig. 5 Distributions of soot nucleation rate under different gravity levels with the peak values indicated. The unit of soot nucleation rate is g/cm^3 s

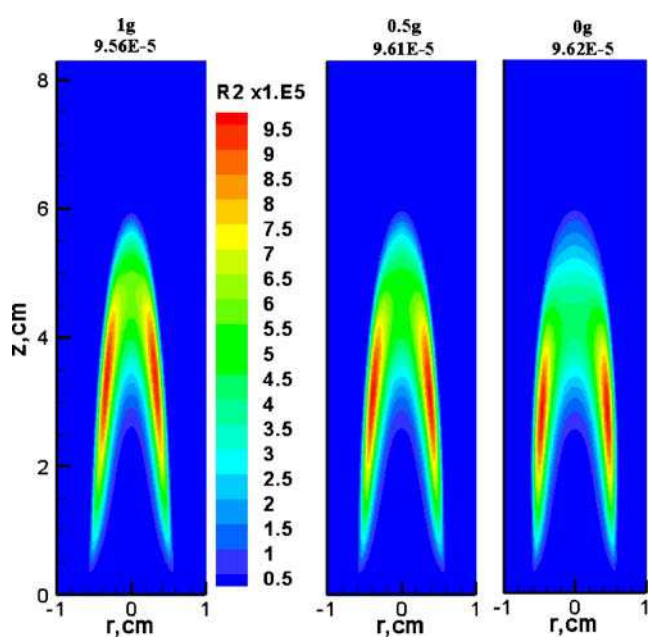

Fig. 6 Distributions of surface growth rate under different gravity levels with the peak values indicated. The unit of surface growth rate is g/cm^3 s

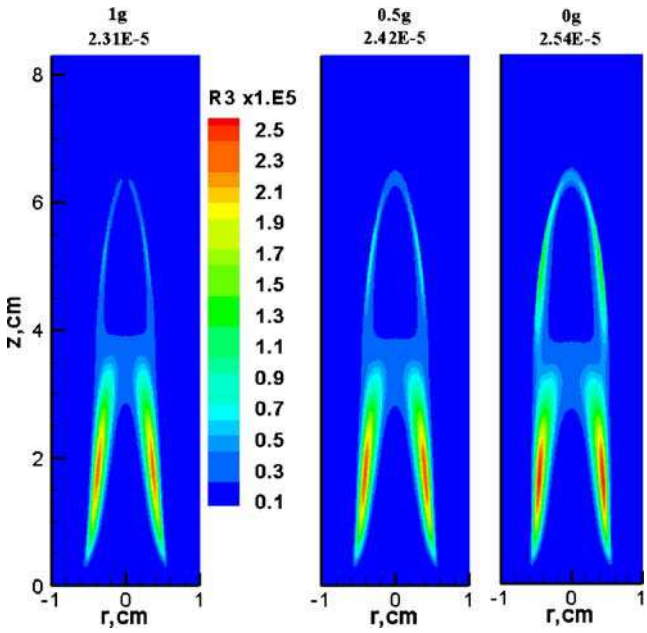

Fig. 7 Distributions of soot oxidation rate by O_2 under different gravity levels with the peak values indicated. The unit of oxidation rate is g/cm^3 s

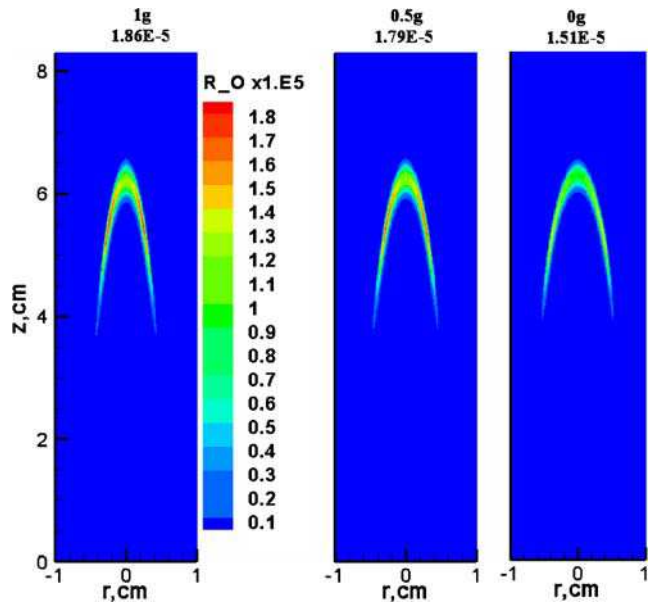

Fig. 9 Distributions of soot oxidation rate by O under different gravity levels with the peak values indicated. The unit of oxidation rate is g/cm^3 s

soot nucleation, surface growth and oxidation processes are also different under different conditions. It is seen from Fig. 5 that the peak soot nucleation rate decreases slightly with the decrease of the gravity level. For each case, most of the soot nucleates at the outer boundary near the flame base within an annular soot layer. As gravity is gradually reduced, the region of high soot nucleation rates moves upstream closer to the burner. Furthermore the nucleation rates in the upper portion of the buoyant flame are greater than those in the non-buoyant flame.

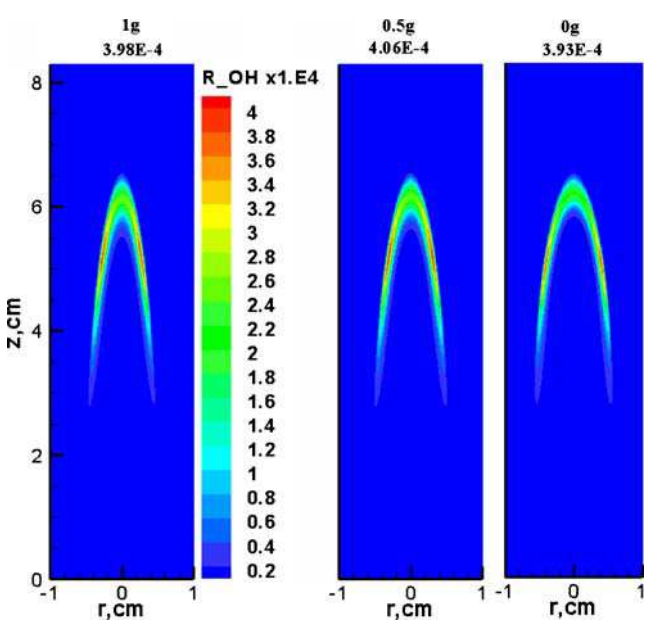

Fig. 8 Distributions of soot oxidation rate by OH under different gravity levels with the peak values indicated. The unit of oxidation rate is g/cm^3 s

The soot surface growth rates shown in Fig. 6 have similar patterns for different gravity cases. The peak soot surface growth rate again increases slightly under reduced gravity. The larger soot volume fractions in the zero gravity flame can be therefore attributed to the longer residence time for soot surface growth. For each case, the soot nucleation and surface growth rate have similar pattern with the distributions of C_2H_2. The soot nucleation and surface growth cease when acetylene is depleted. The area of soot nucleation and surface growth becomes wider and shorter when the influence of gravity is removed.

Soot oxidation by O_2 shown in Fig. 7 occurs in two separate regions: one near the base of the flame and on the fuel-rich side and the other in the upper portion of the flame around the visible envelope. The oxidation by O_2 near the flame base is caused by O_2 leakage into the fuel-rich region through the burner rim, but these oxidation rates are low due to the limited oxygen supply and relatively low soot concentrations. O_2 also contributes to soot oxidation in the post flame region, but at even lower rates. The appearance of two separate regions of soot oxidation by O_2 has also been predicted by Liu et al. (2004) and Smooke et al. (1999) in normal

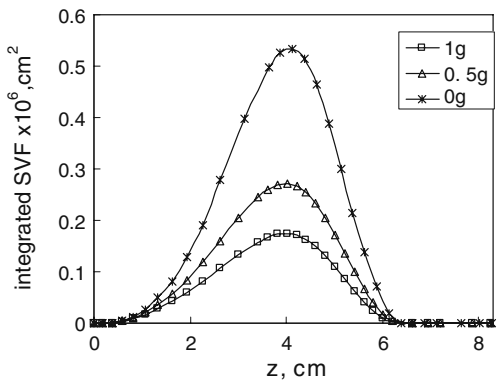

Fig. 10 Distributions of the integrated soot volume fraction under different gravity levels

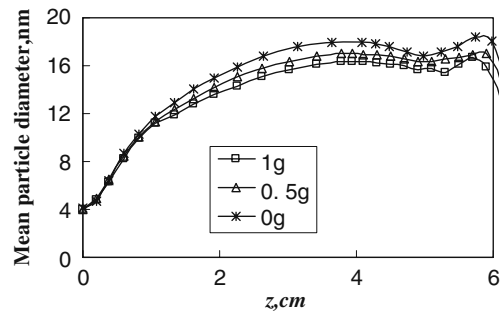

Fig. 12 Predicted mean primary soot particle diameter along the path-line of maximum soot volume fraction at the maximum soot volume fraction under different gravity levels

gravity. In partial and zero gravity flames, soot oxidation patterns are similar to that in normal gravity. The peak soot oxidation by O_2 increases slightly with the decrease of the gravity level. The soot oxidation rate by O_2 in the post flame region for non-buoyant flame is slightly larger than that for normal gravity flame.

Soot oxidation by OH radical shown in Fig. 8 is clearly the dominant mechanism for soot burnout, which has also been observed in many previous studies. The cause of the important role of OH as the principal oxidizing species is its high super-equilibrium level in the flame front. The present results show that in the upper portion of the flame along the centerline, the calculated OH concentration decreases with the decrease of the gravity level, which has a similar variation trend to that of temperature. Such variation in the OH concentration affects the soot oxidation rate by OH so that in regions close to the flame tip the oxidation rate decreases with the decrease of the gravity level.

Soot oxidation by O radical shown in Fig. 9 occurs in a region similar to that for OH, but the rates for the O radical are more than an order of magnitude lower. The oxidation rate by O for non-buoyant flame is obviously lower than that for buoyant flame.

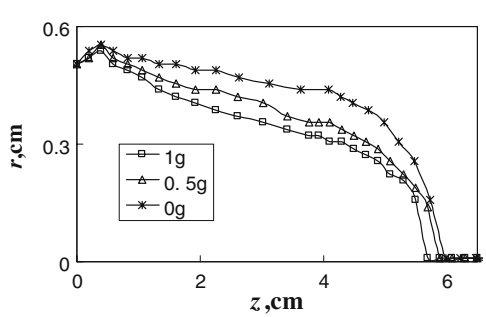

Fig. 11 Path-lines of maximum soot concentration occurrence in different gravity levels

The cross-sectional area integrated soot volume fractions across the flame along the flame height computed as $\int f_v 2\pi r dr$ are shown in Fig. 10 for the various gravitational conditions. It is seen from Fig. 10 that the non-buoyant flame produces much more soot than the buoyant one due to (1) expansion of the flame in the radial direction, which leads to a much larger cross-sectional area of the annular sooting region, and (2) the much longer residence time for soot particle surface growth as a result of the removal of buoyancy-induced convection, Fig. 3, which results in higher soot volume fraction.

The radial location of the maximum soot volume fraction along the axial direction is shown in Fig. 11. The location of the maximum soot volume fraction first moves outwards radially slightly then inwards to the flame axis along the flame height under all gravity levels. At a given flame height, however, the location of the maximum soot volume fraction occurs at a larger radial position as the gravity level decreases. The mean primary soot particle diameter is computed as $(6/\pi)^{1/3}(Y_s/\rho_s N)^{1/3}$. The distributions of the predicted mean primary soot particle diameter under different gravity levels shown in Fig. 12 have similar profiles along the axial height. However, the soot particle size for the non-buoyant flame is greater than that for buoyant flame.

Conclusions

The gravity effects on soot formation have been investigated using detailed numerical calculations in a laminar coflow methane/air diffusion flame at atmospheric pressure. Fully coupled calculations of flow, gas-phase

reactions, soot kinetics, and nongray radiation were conducted. 2D representations of temperature, soot volume fraction, soot nucleation, surface growth and oxidation rates were obtained under different gravity conditions. The computational results reproduce many of the flame phenomena observed in microgravity experiments. Numerical results are consistent with the experimental observations that in microgravity a laminar diffusion flame is taller and wider than its counterpart in normal gravity. The elimination of buoyancy-induced acceleration of flow in microgravity causes a significant reduction in axial velocity and longer residence time, and thus more soot is produced and the radiation cooling effects are enhanced in microgravity. The predicted peak temperature is lower in microgravity as a result of increased radiation heat loss. The predicted soot volume fraction in microgravity is about twice that in normal gravity, which is in quantitative agreement with experimental results. Under different gravity conditions, the location and intensity of soot nucleation, surface growth and oxidation were different, but similar. The predicted results show a significant increase in the overall integrated soot volume fraction in microgravity. The mean primary soot particle diameter increases with decreasing the gravity level.

Acknowledgement Financial support from NSFC under grant no. 59886002, 59986004 and 50976115 is gratefully acknowledged.

References

Aalburg, C., Diez, F.J., Faeth, G.M., Sunderland, P.B., Urban, D.L., Yuan, Z.-G.: Shapes of nonbuoyant round hydrocarbon-fueled laminar-jet diffusion flames in still air. Combust. Flame **142**, 1–16 (2005)

Bahadori, M.Y., Edelman, R.B., Stocker, D.P., Olson, S.L.: Ignition and behavior of laminar gas-jet diffusion flames in microgravity. AIAA J. **28**, 236–244 (1990)

Brahmi, L., Vietoris, T., Rouvreau, S., Joulain, P., David, L., Torero, J.L.: Microgravity laminar diffusion flame in a perpendicular fuel and oxidizer stream configuration. AIAA J. **43**, 1725–1733 (2005)

Fuentes, A., Rouvreau, S., Joulain, P., Vantelon, J.-P., Legros, G., Torero, J.L., Fernandez-Pello, A.C.: Sooting behavior dynamics of a non-buoyant laminar diffusion flame. Combust. Sci. Technol. **179**, 3–19 (2007)

Glassman, I.: Soot formation in combustion processes. Proc. Combust. Inst. **22**, 295–311 (1988)

Greenberg, P.S., Ku, J.C.: Soot volume fraction imaging. Appl. Opt. **36**, 5514–5522 (1997a)

Greenberg, P.S., Ku, J.C.: Soot volume fraction maps for normal and reduced gravity laminar acetylene jet diffusion flames. Combust. Flame **108**, 227–230 (1997b)

Guo, H., Liu, F., Smallwood, G.J., Gülder, Ö.L.: The flame preheating effect on numerical modelling of soot formation in a two-dimensional laminar ethylene-air diffusion flame. Combust. Theory Model. **6**, 173–187 (2002)

Haggard, J.B., Cochran, T.H.: Stable hydrocarbon diffusion flames in a weightless environment. Combust. Sci. Technol. **5**, 291–298 (1972)

Haynes, B.S., Wagner, H.Gg.: Soot formation. Prog. Energy Combust. Sci. **7**, 229–273 (1981)

Kaplan, C.R., Oran, E.S., Kailasanath, K.: Gravitational effects on sooting diffusion flames. Proc. Combust. Inst. **26**, 1301–1309 (1996a)

Kaplan, C.R., Shaddix, C.R., Smyth, K.C.: Computations of enhanced soot production in time-varying. CH_4 /air diffusion flames. Combust. Flame **106**, 392–405 (1996b)

Kong, W., Liu, F.: Numerical study of the effects of gravity on soot formation in laminar coflow methane/air diffusion flames under different air stream velocities. Combust. Theory Model. (2009, in press)

Konsur, B., Megaridis, C.M.: Fuel preheat effects on soot-field structure in laminar gas jet diffusion flames burning in 0-g and 1-g. Combust. Flame **116**, 334–347 (1999)

Ku, J.C., Griffin, D.W., Greenberg, P.S., Roma, J.: Buoyancy-induced differences in soot morphology. Combust. Flame **102**, 216–218 (1995)

Legros, G., Joulain, P., Vantelon, J.-P., Fuentes, A., Bertheau, D., Torero, J.L.: Soot volume fraction measurements in a three-dimensional laminar diffusion flame established in microgravity. Combust. Sci. Technol. **178**, 813–835 (2006)

Legros, G., Fuentes, A., Rouvreau, S., Joulain, P., Porterie, B., Torero, J.L.: Transport mechanisms controlling soot production inside a non-buoyant laminar diffusion flame. Proc. Combust. Inst. **32**, 2461–2470 (2009)

Lin, K.C., Faeth, G.M., Sunderland, P.B., Urban, D.L., Yuan, Z.-G.: Shapes of nonbuoyant round luminous hydrocarbon/air laminar jet diffusion flames. Combust. Flame **116**, 415–431 (1999)

Liu, F., Kong, W.: Experimental observation and numerical modelling of a laminar double coflow methane/air diffusion flame. In: Proceedings of the ASME International Mechanical Engineering Congress and Exposition, IMECE-2007-42745, vol. 6, pp. 761–768. (2008)

Liu, F., Guo, H., Smallwood, G.J., Gülder, Ö.L.: Effects of gas and soot radiation on soot formation in a coflow laminar ethylene diffusion flame. J. Quant. Spectrosc. Radiat. Transfer **73**, 409–421 (2002)

Liu, F., Guo, H., Smallwood, G.J.: Effects of radiation model on the modeling of a laminar coflow methane/air diffusion flame. Combust. Flame **138**, 136–154 (2004)

Liu, F., Smallwood, G.J., Kong, W.: Structure and soot formation characteristics of a double coflow methane diffusion flame. In: 9th AIAA/ASME Joint Thermophysics and Heat Transfer Conference Proceedings AIAA-2006-3285, vol. 2, pp. 1175–1186 (2006)

Megaridis, C.M., Griffin, D.W., Konsur, B.: Soot-field structure in laminar soot-emitting microgravity nonpremixed flames. Proc. Combust. Inst. **26**, 1291–1299 (1996)

Smith, G.P., Golden, D.M., Frenklach, M., Moriarty, N.W., Eiteneer, B., Goldenberg, M., Bowman, C.T., Hanson, R.K., Song, S., Gardiner, W.C. Jr., Lissianski, V.V., Qin, Z.: http://www.me.berkeley.edu/gri-mech/. Accessed 17 Dec. 2009

Smooke, M.D., McEnally, C.S., Pfefferle, L.D., Hall, R.J., Colket, M.B.: Computational and experimental study of soot formation in a coflow, laminar diffusion flame. Combust. Flame **117**, 117–139 (1999)

Smooke, M.D., Xu, Y., Zurn, R.M., Lin, P., Frank, J.H., Long, M.B.: Computational and experimental study of OH and CH radicals in axisymmetric laminar diffusion flames. Proc. Combust. Inst. **24**, 813–822 (1992)

Smooke, M.D., Ern, A., Tanoff, M.A., Valdati, B.A., Mohammed, R.K., Marran, D.F., Long, M.B.: Computational and experimental study of no in an axisymmetric laminar diffusion flame. Proc. Combust. Inst. **26**, 2161–2170 (1996)

Soufiani, A., Taine, J.: High temperature gas radiative property parameters of statistical narrow-band model for H_2O, CO_2 and CO, and correlated-K model for H_2O and CO_2. Int. J. Heat Mass Transfer **40**, 987–991 (1997)

Sunderland, P.B., Mortazavi, S., Faeth, G.M., Urban, D.L.: Laminar smoke points of nonbuoyant jet diffusion flames. Combust. Flame **96**, 97–103 (1994)

Urban, D.L., Yuan, Z.-G., Sunderland, P.B., Lin, K.-C., Dai, Z., Faeth, G.M.: Smoke-point properties of non-buoyant round laminar jet diffusion flames. Proc. Combust. Inst. **28**, 1965–1972 (2000)

Vietoris, T., Ellzey, J.L., Joulain, P., Mehta, S.N., Torero, J.L.: Laminar diffusion flame in microgravity: the results of the minitexus 6 sounding rocket experiment. Proc. Combust. Inst. **28**, 2883–2889 (2000)

Walsh, K.T., Long, M.B., Tanoff, M.A., Smooke, M.D.: Experimental and computational study of CH, CH*, and OH* in an axisymmetric laminar diffusion flame. Proc. Combust. Inst. **27**, 615–623 (1998)

Walsh, K.T., Fielding, J., Smooke, M.D., Long, M.B.: Experimental and computational study of temperature, species, and soot in buoyant and non-buoyant coflow laminar diffusion flames. Proc. Combust. Inst. **28**, 1973–1979 (2000)